Physics Letters B 833 (2022) 137342

Contents lists available at ScienceDirect

Physics Letters B

www.elsevier.com/locate/physletb

# Electroweak corrections to dark matter direct detection in the dark singlet phase of the N2HDM

Seraina Glaus [a,b], Margarete Mühlleitner [a], Jonas Müller [a], Shruti Patel [a,b], Rui Santos [c,d,*]

[a] Institute for Theoretical Physics, Karlsruhe Institute of Technology, 76128 Karlsruhe, Germany
[b] Institute for Nuclear Physics, Karlsruhe Institute of Technology, 76344 Karlsruhe, Germany
[c] Centro de Física Teórica e Computacional, Faculdade de Ciências, Universidade de Lisboa, Campo Grande, Edifício C8, 1749-016 Lisboa, Portugal
[d] ISEL - Instituto Superior de Engenharia de Lisboa, Instituto Politécnico de Lisboa, 1959-007 Lisboa, Portugal

ARTICLE INFO

*Article history:*
Received 29 April 2022
Received in revised form 3 July 2022
Accepted 20 July 2022
Available online 25 July 2022
Editor: J. Hisano

ABSTRACT

Direct detection experiments are the only way to obtain indisputable evidence of the existence of dark matter (DM) in the form of a particle. These experiments have been used to probe many extensions of the Standard Model (SM) that provide DM candidates. Experimental results like the latest ones from XENON1T lead to severe constraints in the parameter space of many of the proposed models. In a simple extension of the SM, the addition of a complex singlet to the SM content, one-loop corrections need to be taken into account because the tree-level cross section is proportional to the DM velocity, and therefore negligible. In this work we study the case of a DM particle with origin in a singlet but in a larger framework of an extension by an extra doublet together with the extra singlet providing the DM candidate. We show that in the region of interest of the present and future direct detection experiments, electroweak corrections are quite stable with a $K$-factor very close to one.



## 1. Introduction

The only way to unmistakably identify a dark matter (DM) particle is in direct detection experiments. In the mass region of the so-called Weekly Interacting Massive Particles (WIMPs) the latest and most restrictive constraints were obtained by the PandaX-4T [1] and by the XENON1T collaboration [2,3] (we will include both bounds in our plots). In this type of experiments, when DM interacts with Xenon it creates light and electric charge and these signals provide information about the energy and location of the initial collision. Since direct detection experiments play the major role in probing the WIMP region it is important to understand in great detail the DM-nucleon cross sections in the different models. There is a particularly interesting case, the one of the extension of the SM by a complex singlet that leads to a tree-level DM-nucleon cross section proportional to the DM velocity and therefore to a negligible rate [4]. The calculation of the electroweak corrections to DM-nucleon scattering in this model was performed in [5–7] and shown to be several orders of magnitude above the tree-level result.

In previous works we have also calculated the electroweak corrections [8,9] in a vector DM model [10]. In this case the tree-level cross section is not negligible and electroweak corrections, in the region not excluded by XENON1T/PandaX-4T, are quite stable with a $K$-factor close to 1 ($K = \sigma_{\rm NLO}/\sigma_{\rm LO}$ - the ratio of the next-to-leading order to the leading order cross section). In this letter we discuss a scenario where the DM candidate originates from a singlet but now within the larger framework of the Dark Singlet Phase (DSP) [11,12] of the next to 2-Higgs Doublet Model (N2HDM). The first point to note is that in this case there is no tree-level cancellation. Hence, the leading order cross section is not negligible. The main question we would like to answer is if the corrections are still stable and not too large when the parameter space of the visible sector is enlarged which is the case of the DSP of the N2HDM. The DM candidate is singlet-like but the visible sector is now a $Z_2$ symmetric 2HDM, with a new set of parameters and extra contributions to the electroweak corrections. As we have discussed in great detail all the steps of the calculations in our previous works [7–9] and also because there are no major changes in the methodology we will whenever possible refer the reader to those works and will just focus on the differences for the model under study.

* Corresponding author.
*E-mail addresses:* milada.muehlleitner@kit.edu (M. Mühlleitner), rasantos@fc.ul.pt (R. Santos).

https://doi.org/10.1016/j.physletb.2022.137342

The outline of the letter is as follows. In section 2, we will introduce the DSP of the N2HDM together with our notation. Section 3 contains a brief description of the renormalization procedure used in this work. In section 4 we calculate the electroweak corrections to the spin-independent direct detection cross section. In section 5, the results are presented and discussed. Finally, we present our conclusions in section 6.

## 2. The dark singlet phase of the N2HDM

The model considered in this work is the DSP of the N2HDM [13–15]. The Higgs sector of the SM is extended by one complex $SU(2)_L$ doublet with hypercharge +1, and one real $SU(2)_L$ singlet with hypercharge 0. We focus on a particular phase of the four possible dark phases of the N2HDM, the DSP, where the singlet field has a vanishing vacuum expectation value (VEV) and does not couple to the SM fields, making it a DM candidate. A detailed discussion of the different dark matter phases of the N2HDM can be found in [11,16]. The Yukawa version of the model is type I meaning that all quarks and leptons couple to only one of the doublets. The Higgs potential is simplified by requiring invariance under the two $\mathbb{Z}_2$ symmetries,

$$\mathbb{Z}_2^{(1)}: \quad \Phi_1 \to -\Phi_1, \quad \Phi_2 \to \Phi_2, \quad \Phi_S \to \Phi_S\,, \tag{1}$$

$$\mathbb{Z}_2^{(2)}: \quad \Phi_1 \to \Phi_1, \quad \Phi_2 \to \Phi_2, \quad \Phi_S \to -\Phi_S\,, \tag{2}$$

which allows us to write the most general CP-conserving and renormalizable scalar potential invariant under these $\mathbb{Z}_2$ symmetries as

$$\begin{aligned} V_{\text{scalar}} = {} & m_{11}^2 \Phi_1^\dagger \Phi_1 + m_{22}^2 \Phi_2^\dagger \Phi_2 + \frac{\lambda_1}{2}\left(\Phi_1^\dagger \Phi_1\right)^2 + \frac{\lambda_2}{2}\left(\Phi_2^\dagger \Phi_2\right)^2 \\ & + \lambda_3 \Phi_1^\dagger \Phi_1 \Phi_2^\dagger \Phi_2 + \lambda_4 \Phi_1^\dagger \Phi_2 \Phi_2^\dagger \Phi_1 + \frac{\lambda_5}{2}\left[\left(\Phi_1^\dagger \Phi_2\right)^2 + \text{h.c.}\right] \\ & + \frac{1}{2} m_S^2 \Phi_S^2 + \frac{\lambda_6}{8}\Phi_S^4 + \frac{\lambda_7}{2}\Phi_1^\dagger \Phi_1 \Phi_S^2 + \frac{\lambda_8}{2}\Phi_2^\dagger \Phi_2 \Phi_S^2\,, \end{aligned} \tag{3}$$

with three real mass dimension parameters $m_{11}^2, m_{22}^2, m_s^2$ and eight real dimensionless parameters $\lambda_1 \cdots \lambda_8$. The symmetry $\mathbb{Z}_2^{(1)}$ is spontaneously broken by the doublet VEV. In the DSP, both doublets acquire VEVs but the singlet VEV vanishes which leaves the symmetry $\mathbb{Z}_2^{(2)}$ unbroken. After electroweak symmetry breaking (EWSB) the doublet and singlet fields can be parametrized in terms of the VEVs $v_1$ and $v_2$, and component fields as

$$\Phi_1 = \begin{pmatrix} \phi_1^+ \\ \frac{1}{\sqrt{2}}(v_1 + \rho_1 + i\eta_1) \end{pmatrix}, \qquad \Phi_2 = \begin{pmatrix} \phi_2^+ \\ \frac{1}{\sqrt{2}}(v_2 + \rho_2 + i\eta_2) \end{pmatrix}, \qquad \Phi_s = \rho_s\,, \tag{4}$$

where $\phi_1^+, \phi_2^+$ are complex charged fields, $\rho_1, \rho_2, \rho_s$ $\eta_1$ and $\eta_2$ are neutral fields. After EWSB, the CP-even fields $\rho_1$ and $\rho_2$ mix and give rise to the CP-even mass eigenstates $h_1$ and $h_2$ defined such that $m_{h_1} \leq m_{h_2}$, and either $h_1$ or $h_2$ can be identified with the 125 GeV SM Higgs boson. Similarly $\eta_1$ and $\eta_2$ mix to give a pseudoscalar mass eigenstate $A$ and the neutral Goldstone boson $G^0$. Finally, $\phi_1^+, \phi_2^+$ mix to give a charged Higgs $H^+$ and the charged Goldstone boson $G^+$. The singlet field $\rho_s$ does not mix with any of the doublet fields, nor does it couple to any SM particles. Moreover, the unbroken $\mathbb{Z}_2^{(2)}$ symmetry gives rise to a dark parity, such that $\rho_s \equiv \chi$ with mass $m_\chi$ emerges as a DM candidate in the model.

The mass eigenstates can be expressed in terms of the gauge eigenstates via rotation matrices as follows,

$$\begin{pmatrix} h_1 \\ h_2 \\ \chi \end{pmatrix} = R_\alpha \begin{pmatrix} \rho_1 \\ \rho_2 \\ \rho_s \end{pmatrix}, \qquad \begin{pmatrix} G^0 \\ A \end{pmatrix} = U_\beta \begin{pmatrix} \eta_1 \\ \eta_2 \end{pmatrix}, \qquad \begin{pmatrix} G^\pm \\ H^\pm \end{pmatrix} = U_\beta \begin{pmatrix} \phi_1^\pm \\ \phi_2^\pm \end{pmatrix}, \tag{5}$$

where the rotation matrices are parametrized as[1]

$$R_\alpha = \begin{pmatrix} \cos\alpha & \sin\alpha & 0 \\ -\sin\alpha & \cos\alpha & 0 \\ 0 & 0 & 1 \end{pmatrix}, \qquad U_\beta = \begin{pmatrix} \cos\beta & \sin\beta \\ -\sin\beta & \cos\beta \end{pmatrix}. \tag{6}$$

The VEVs of the two doublets are related to the SM VEV ($v \approx 246.22$ GeV) as

$$v_1 = v\cos\beta\,, \qquad v_2 = v\sin\beta\,, \tag{7}$$

with $v = 2m_W/g$, where $m_W$ is the mass of the $W^\pm$ boson.

Further details on the minimization conditions can be found in [11,12]. The final set of independent input parameters chosen is

$$v\,, \alpha\,, \tan\beta\,, m_\chi\,, m_{h_1}\,, m_{h_2}\,, m_A\,, m_{H^\pm}\,, \lambda_6\,, \lambda_7\,, \lambda_8\,. \tag{8}$$

[1] Note the different parametrization of $R_\alpha$ compared to [11,12].

## 3. Renormalization of the model

In the following, we present the renormalization of the N2HDM DSP in order to calculate the electroweak (EW) corrections to the scattering process of the scalar DM particle $\chi$ with a nucleon. We follow the prescription presented in [17] by adapting the renormalization of the unbroken phase of the N2HDM to our scenario. This is done by taking the limit $v_s = \alpha_2 = \alpha_3 = 0$ and by additionally renormalizing the parameters $\lambda_7$ and $\lambda_8$, which are the ones that enter our calculation.

The bare input parameters $p_0$ defined in Eq. (8) are expressed in terms of the renormalized parameters $p$ and their respective counterterms $\delta p$ as

$$p_0 = p + \delta p\,, \tag{9}$$

whereas bare fields $\phi_0$ are expressed in terms of the renormalized fields $\phi$ and the wave-function renormalization factors (WFRs) $Z_\phi$ as

$$\phi_0 = \sqrt{Z_\phi}\phi \tag{10}$$

where $Z_\phi$ is a matrix in case the fields mix at one-loop. The renormalization conditions define the finite parts of the counterterms. In this work, we will use the on-shell (OS) renormalization scheme to fix the renormalization constants for the masses and fields. The tadpoles are treated in the Fleischer and Jegerlehner (FJ) [18] scheme. A detailed description of the scheme and its consequences for gauge independence can be found in [17,19–21]. In the following sections we just present a brief description of the renormalization of the model sector by sector, giving the expressions required for the renormalization of the direct detection process $\chi p \to \chi p$.

### 3.1. Scalar sector

In the DSP of the N2HDM, after EWSB there are four neutral scalars (two CP-even, one CP-odd and the DM candidate $\chi$) and one charged Higgs pair. The OS conditions for the physical Higgs states result in the following mass counterterms,

$$\begin{aligned}
&\delta m^2_{h_i} = \mathrm{Re}[\Sigma^{\mathrm{tad}}_{h_i h_i}(m^2_{h_i})]\,,\ i \in \{1,2\}, \qquad \delta m^2_\chi = \mathrm{Re}[\Sigma^{\mathrm{tad}}_{\chi\chi}(m^2_\chi)]\,,\\
&\delta m^2_A = \mathrm{Re}[\Sigma^{\mathrm{tad}}_{AA}(m^2_A)]\,, \qquad \delta m^2_{H^\pm} = \mathrm{Re}[\Sigma^{\mathrm{tad}}_{H^\pm H^\pm}(m^2_{H^\pm})]\,,
\end{aligned} \tag{11}$$

where $\Sigma^{\mathrm{tad}}(p^2)$ are the self-energies containing all tadpole topologies. Since the tadpoles are absorbed into the self-energies, explicit tadpole counterterms do not appear in the mass counterterms [17]. The fields are renormalized in terms of the WFR constants $\delta Z_{\phi_i\phi_j}$ as

$$\begin{pmatrix}\phi_i\\ \phi_j\end{pmatrix} \to \begin{pmatrix} 1+\frac{1}{2}\delta Z_{\phi_i\phi_i} & \frac{1}{2}\delta Z_{\phi_i\phi_j}\\ \frac{1}{2}\delta Z_{\phi_j\phi_i} & 1+\frac{1}{2}\delta Z_{\phi_j\phi_j}\end{pmatrix}\begin{pmatrix}\phi_i\\ \phi_j\end{pmatrix}, \tag{12}$$

where $\{\phi_i,\phi_j\} = \{h_1,h_2\},\{G,A\}$ or $\{G^\pm,H^\pm\}$. We will just show explicitly the 2×2 WFR matrices $\delta Z_{\phi_i,\phi_j}$ for the case $\{h_i,h_j\}$ which reads

$$\begin{pmatrix}\delta Z_{h_1h_1} & \delta Z_{h_1h_2}\\ \delta Z_{h_2h_1} & \delta Z_{h_1h_1}\end{pmatrix} = \begin{pmatrix} -\mathrm{Re}\left.\frac{\partial\Sigma^{\mathrm{tad}}_{h_1h_1}(p^2)}{\partial p^2}\right|_{p^2=m^2_{h_1}} & 2\frac{\mathrm{Re}\left[\Sigma^{\mathrm{tad}}_{h_1h_2}(m^2_{h_2})\right]}{m^2_{h_1}-m^2_{h_2}}\\ 2\frac{\mathrm{Re}\left[\Sigma^{\mathrm{tad}}_{h_2h_1}(m^2_{h_1})\right]}{m^2_{h_2}-m^2_{h_1}} & -\mathrm{Re}\left.\frac{\partial\Sigma^{\mathrm{tad}}_{h_2h_2}(p^2)}{\partial p^2}\right|_{p^2=m^2_{h_2}}\end{pmatrix},$$

and the other two cases are obtained by replacing $\{h_1,h_2\}$ by $\{G,A\}$ and $\{G^\pm,H^\pm\}$.

Finally the field strength renormalization for the DM particle $\chi$ is expressed in terms of its self-energy $\Sigma_{\chi\chi}(p^2)$ as

$$\delta Z_{\chi\chi} = -\mathrm{Re}\left.\frac{\partial\Sigma^{\mathrm{tad}}_{\chi\chi}(p^2)}{\partial p^2}\right|_{p^2=m^2_\chi}. \tag{13}$$

### 3.2. Gauge sector

The gauge sector of the model is renormalized through OS conditions. The masses, couplings and fields are expressed in terms of their counterterms as[2]

$$m^2_W \to m^2_W + \delta m^2_W\,, \quad m^2_Z \to m^2_Z + \delta m^2_Z\,, \tag{14}$$

$$e \to e + \delta Z_e\,, \quad g \to g + \delta g\,, \tag{15}$$

$$W^\pm \to \left(1+\frac{1}{2}\delta Z_{WW}\right)W^\pm\,, \tag{16}$$

$$\begin{pmatrix}Z\\ \gamma\end{pmatrix} \to \begin{pmatrix} 1+\frac{1}{2}\delta Z_{ZZ} & \frac{1}{2}\delta Z_{Z\gamma}\\ \frac{1}{2}\delta Z_{\gamma Z} & 1+\frac{1}{2}\delta Z_{\gamma\gamma}\end{pmatrix}\begin{pmatrix}Z\\ \gamma\end{pmatrix}, \tag{17}$$

[2] The choice of the $\{\alpha \equiv e^2/(4\pi), m_W, m_Z\}$ scheme instead of the $\{G_F, m_W, m_Z\}$ scheme is a pragmatic one as it allows us to make link to our previously computed electroweak corrections of the N2HDM Higgs decays [22] for future further investigations in connection with LHC phenomenology. The induced difference between the two schemes is of higher order and can be expected to be negligible compared to the effects investigated here [22,23].

where $m_W$ and $m_Z$ are the $W$ and $Z$ boson masses, respectively, $e$ is the electric charge and $g$ is the weak $SU(2)_L$ coupling. The OS conditions for the masses give rise to the counterterms

$$\delta m_W^2 = \mathrm{Re}\,\Sigma_{WW}^{\mathrm{tad},T}(m_W^2) \quad \text{and} \quad \delta m_Z^2 = \mathrm{Re}\,\Sigma_{ZZ}^{\mathrm{tad},T}(m_Z^2)\,, \tag{18}$$

where the superscript $T$ indicates the transverse part of the self-energy, which also includes tadpole contributions. The counterterm for the electric charge is fixed in the Thomson limit as in the SM and is expressed in terms of the Weinberg angle $\theta_W$ as

$$\delta Z_e = \frac{1}{2}\left.\frac{\partial \Sigma_{\gamma\gamma}^T(k^2)}{\partial p^2}\right|_{p^2=0} + \frac{\sin\theta_W}{\cos\theta_W}\frac{\Sigma_{\gamma Z}^T(0)}{m_Z^2}\,. \tag{19}$$

Using the above expression we can then fix the counterterm $\delta g$ as

$$\frac{\delta g}{g} = \delta Z_e + \frac{1}{2}\frac{1}{m_Z^2 - m_W^2}\left(\delta m_W^2 - \delta m_Z^2 \cos^2\theta_W\right)\,. \tag{20}$$

Finally, the WFR constants for the gauge fields are given by

$$\delta Z_{WW} = -\mathrm{Re}\left.\frac{\partial \Sigma_{WW}^{\mathrm{tad},T}(p^2)}{\partial p^2}\right|_{p^2=m_W^2}\,, \tag{21}$$

$$\begin{pmatrix} \delta Z_{ZZ} & \delta Z_{Z\gamma} \\ \delta Z_{\gamma Z} & \delta Z_{\gamma\gamma} \end{pmatrix} = \begin{pmatrix} -\mathrm{Re}\left.\frac{\partial \Sigma_{ZZ}^{\mathrm{tad},T}(p^2)}{\partial p^2}\right|_{p^2=m_Z^2} & 2\frac{\Sigma_{Z\gamma}^{\mathrm{tad},T}(0)}{m_Z^2} \\ -2\mathrm{Re}\frac{\Sigma_{Z\gamma}^{\mathrm{tad},T}(m_Z^2)}{m_Z^2} & -\left.\frac{\partial \Sigma_{\gamma\gamma}^{\mathrm{tad},T}(p^2)}{\partial p^2}\right|_{p^2=0} \end{pmatrix}\,. \tag{22}$$

### 3.3. Quark sector

In the quark sector the OS scheme is applied for each quark. The renormalized quark fields are expressed in terms of their left- and right-handed components, with counterterms for each component as follows

$$q_{L/R} \to \left(1 + \frac{1}{2}\delta Z_{qq}^{L/R}\right) q\,, \tag{23}$$

with $q \in \{u, d, s, c, b, t\}$. In order to fix the counterterms we need to define the structure of the quark self-energies,

$$\Sigma_q(p^2) = \not{p}\,\Sigma_{qq}^L(p^2)P_L + \not{p}\,\Sigma_{qq}^R(p^2)P_R + m_f(P_L + P_R)\Sigma_{qq}^S(p^2)\,, \tag{24}$$

where the self-energy superscripts $L, R$ and $S$ respectively correspond to the left-handed, right-handed and scalar parts of the quark self-energies, and $P_{L,R}$ are the left- and right-handed projectors. Using the above expression the quark WFR constants and mass counterterms in terms of the self-energies containing the tadpole topologies, are defined as

$$\begin{aligned} \delta Z_q^{L/R} &= -\,\mathrm{Re}\,\Sigma_q^{\mathrm{tad},L/R}(m_q^2) - m_q^2\frac{\partial}{\partial p^2}\mathrm{Re}\left(\Sigma_{qq}^{\mathrm{tad},L/R}(p^2) + \Sigma_{qq}^{\mathrm{tad},R/L}(p^2) + 2\Sigma_{qq}^{\mathrm{tad},S}(p^2)\right)\Big|_{p^2=m_q^2}\,, \\ \frac{\delta m_q}{m_q} &= \frac{1}{2}\mathrm{Re}\left[\Sigma_{qq}^{\mathrm{tad},L}(m_q^2) + \Sigma_{qq}^{\mathrm{tad},R}(m_q^2) + 2\Sigma_{qq}^{\mathrm{tad},S}\right]\,. \end{aligned} \tag{25}$$

### 3.4. Renormalization of the mixing angles

Following the renormalization prescription for mixing angles in the 2HDM, the angles $\alpha$ and $\beta$ are renormalized as proposed in [17,24,25]. The scheme connects $\delta\alpha$ and $\delta\beta$ to the off-diagonal WFR constants of the scalar sector. Following again [17] the angle counterterms are

$$\delta\alpha = \frac{1}{4}\left(\delta Z_{h_1h_2} - \delta Z_{h_2h_1}\right)\,. \tag{26}$$

The counterterm for $\delta\beta$ can be derived either from the charged sector or the CP-odd sector using the same steps, and therefore we have two possible expressions for $\delta\beta$ given by

$$\delta\beta^{(1)} = \frac{1}{4}(\delta Z_{G^\pm H^\pm} - \delta Z_{H^\pm G^\pm}) \tag{27}$$

and

$$\delta\beta^{(2)} = \frac{1}{4}(\delta Z_{G^0A} - \delta Z_{AG^0})\,. \tag{28}$$

### 3.5. Renormalization of $\lambda_7$ and $\lambda_8$

We are left with the parameters $\lambda_7$ and $\lambda_8$ to complete the renormalization of the model. We will use a process-dependent scheme with the on-shell decays $h_i \to \chi\chi$ $(i = 1, 2)$. The NLO amplitude $\mathcal{A}^{NLO}$ consists of the LO decay amplitude $\mathcal{A}^{LO}$, the vertex corrections $\mathcal{A}^{VC}$ and the counterterm amplitude $\mathcal{A}^{CT}$,

$$\mathcal{A}^{NLO}_{h_i} = \mathcal{A}^{LO}_{h_i} + \mathcal{A}^{VC}_{h_i} + \mathcal{A}^{CT}_{h_i}, \tag{29}$$

where the index $h_i$ denotes the decaying particle. The renormalization condition is such that we force the LO decay width to be equal to NLO decay width. With the Higgs coupling $C_{\chi\chi h_i}$ between $h_i$ and two DM particles given by

$$C_{\chi\chi h_i} = \begin{cases} (\lambda_7 \cos\beta\cos\alpha + \lambda_8 \sin\beta\sin\alpha)\frac{2m_W}{g}, & i = 1 \\ (-\lambda_7 \cos\beta\sin\alpha + \lambda_8 \sin\beta\cos\alpha)\frac{2m_W}{g}, & i = 2 \end{cases} \tag{30}$$

this condition gives rise to a system of equations for $\delta\lambda_7$ and $\delta\lambda_8$ such that

$$\begin{aligned} \frac{\partial\mathcal{A}^{LO}_{h_1}}{\partial\lambda_7}\delta\lambda_7 + \frac{\partial\mathcal{A}^{LO}_{h_1}}{\partial\lambda_8}\delta\lambda_8 = -\Bigg(&\mathcal{A}^{VC}_{h_1} + \frac{1}{2}(\mathcal{A}^{LO}_{h_2}\delta Z_{h_2h_1} + \mathcal{A}^{LO}_{h_1}\delta Z_{h_1h_1} + 2\mathcal{A}^{LO}_{h_1}\delta Z_{\chi\chi}) \\ &+ \frac{\partial\mathcal{A}^{LO}_{h_1}}{\partial m_W^2}\delta m_W^2 + \frac{\partial\mathcal{A}^{LO}_{h_1}}{\partial g}\delta g + \frac{\partial\mathcal{A}^{LO}_{h_1}}{\partial\alpha}\delta\alpha + \frac{\partial\mathcal{A}^{LO}_{h_1}}{\partial\beta}\delta\beta\Bigg) \end{aligned} \tag{31}$$

$$\begin{aligned} \frac{\partial\mathcal{A}^{LO}_{h_2}}{\partial\lambda_7}\delta\lambda_7 + \frac{\partial\mathcal{A}^{LO}_{h_2}}{\partial\lambda_8}\delta\lambda_8 = -\Bigg(&\mathcal{A}^{VC}_{h_2} + \frac{1}{2}(\mathcal{A}^{LO}_{h_1}\delta Z_{h_1h_2} + \mathcal{A}^{LO}_{h_2}\delta Z_{h_2h_2} + 2\mathcal{A}^{LO}_{h_2}\delta Z_{\chi\chi}) \\ &+ \frac{\partial\mathcal{A}^{LO}_{h_2}}{\partial m_W^2}\delta m_W^2 + \frac{\partial\mathcal{A}^{LO}_{h_2}}{\partial g}\delta g + \frac{\partial\mathcal{A}^{LO}_{h_2}}{\partial\alpha}\delta\alpha + \frac{\partial\mathcal{A}^{LO}_{h_2}}{\partial\beta}\delta\beta\Bigg), \end{aligned} \tag{32}$$

and this concludes our renormalization programme. We can now proceed to the calculation of the EW corrections.

## 4. Electroweak corrections to the SI cross section

The spin-independent (SI) DM-nucleon cross section can be written in terms of an effective coupling, $\alpha_n$, such that

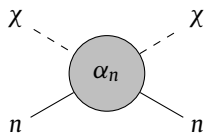


$$= i\mathcal{A}_n = i\alpha_n\bar{u}_n u_n = i\cdot 2m_n\alpha_n, \tag{33}$$

where $\bar{u}_n u_n = 2m_n$ ($m_n$ is the nucleon mass) because we assume that the velocity of the DM particle is negligibly small. With this definition the DM-nucleon cross section takes the form

$$\sigma_n = \frac{1}{4\pi}\left(\frac{m_n}{m_n + m_\chi}\right)^2 |\alpha_n|^2, \tag{34}$$

where $m_\chi$ is the DM mass. As the nucleon is a bound state, the DM-nucleon coupling receives contributions both from valence quarks ($q = u, d, s$) and from the gluons. The SI DM-nucleon cross section is calculated using a parton basis, with the operators considered in the non-relativistic limit. Its most general form is given by [26]

$$\mathcal{L}_{\text{eff}} = \sum_q C_S^q \mathcal{O}_S^q + C_S^g \mathcal{O}_S^g + \sum_q C_T^q \mathcal{O}_T^q, \tag{35}$$

with the operators

$$\mathcal{O}_S^q = m_q \chi^2 \bar{q} q, \tag{36a}$$

$$\mathcal{O}_S^g = \frac{\alpha_s}{\pi}\chi^2 G^a_{\mu\nu} G^{a\mu\nu}, \tag{36b}$$

$$\mathcal{O}_T^q = \frac{1}{m_\chi^2}\chi^2 i\partial^\mu i\partial^\nu \underbrace{\frac{1}{2}i\bar{q}\left(\partial_\mu\gamma_\nu + \partial_\nu\gamma_\nu - \frac{1}{2}g_{\mu\nu}\partial\!\!\!/\right)}_{\equiv\mathcal{O}^q_{\mu\nu}} q, \tag{36c}$$

which are built with the DM field $\chi$, the quark spinor $q$ and the gluon field strength tensor $G^a_{\mu\nu}$; $\alpha_s$ is the strong coupling constant. The quark-DM interaction is encoded in the operator $\mathcal{O}_S^q$ while the gluon-DM interaction is encoded in $\mathcal{O}_S^g$. Finally, the twist-2 operator $\mathcal{O}^q_{\mu\nu}$ also contributes to the SI cross section. The expectation values of the operators in Eq. (36) are written as [27–29]

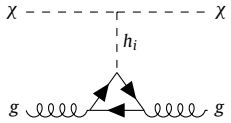


**Fig. 1.** Interaction of a DM particle and a gluon via a Higgs boson mediator and a quark loop.

$$\langle n|\, m_q \bar{q} q\, |n\rangle \equiv m_n f_q^n\,, \tag{37a}$$

$$\langle n|\, -\frac{\alpha_s}{12\pi} G^a_{\mu\nu} G^{a\mu\nu}\, |n\rangle \equiv \frac{2}{27} m_n f_g^n\,, \tag{37b}$$

where the nucleon matrix elements $f_q^n$ and $f_g^n$ are determined by lattice calculations. Their numerical values are given in Appendix A. The QCD trace anomaly relates the heavy quark $Q = b, c, t$ operators with the gluon field strength tensor [29]

$$m_Q\, \bar{Q}\, Q \to -\frac{\alpha_s}{12\pi} G^a_{\mu\nu} G^{a\mu\nu}\,, \tag{38}$$

corresponding to the Feynman diagram in Fig. 1 and can therefore be determined by first calculating the (heavy) external quark process and then using Eq. (38) to determine the effective gluon interaction. These amplitudes are then used to the extract the Wilson coefficients $C_S^g$.

The DM nucleon cross section $\sigma_n$ is given at NLO by

$$\sigma_n = \frac{1}{\pi}\left(\frac{m_n}{m_\chi + m_n}\right)^2 \left(|f_n^{LO}|^2 + 2Re\left(f_n^{LO} f_n^{NLO}\right)\right) \tag{39}$$

where, according to the previous discussion, the LO and NLO form factors are given as

$$f_n^{LO} = m_n C_S^q \left(\sum_{q=u,d,s} f_q^n + \sum_{q=c,b,t} \frac{2}{27} f_g^n\right)\,, \tag{40}$$

$$f_n^{NLO} = m_n \left(\sum_{q=u,d,s} C_S^{q,NLO} f_q^n + \sum_{q=u,d,s,c,b} \frac{3}{4}\left(q(2) + \bar{q}(2)\right) C_T^q - \frac{8\pi}{9\alpha_s} C_S^g f_g^n\right)\,. \tag{41}$$

We will neglect the term proportional to $C_S^g$ because the matching in Eq. (38) cannot be used at EW NLO. As discussed in [7], taking into account the EW NLO corrections of the gluon contributions would require a proper mixed QCD-EW matching of the QCD trace anomaly.[3] Therefore the NLO contributions considered are

$$C_S^{q,NLO} = f_q^{uV} + f_q^{lV} + f_q^{med} + f_q^{box}\,, \tag{42}$$

$$C_T^q = g_q^{box}\,. \tag{43}$$

Here $f_q^i$ are the Wilson coefficients from the upper vertex corrections, lower vertex corrections, mediator corrections and the box contributions. The $g_q^{box}$ are the box contributions proportional to the second momenta of the quarks $q^n(2)$. The values for $q^n(2)$ are also given in Appendix A.

### 4.1. Upper vertex corrections

For the extraction of the Wilson coefficients of the upper vertex the one-loop corrections to the coupling $\chi\chi h_i$ $(i = 1, 2)$ need to be calculated. For this purpose $\chi$ is taken on-shell and it is assumed that the momentum transfer goes to zero. Thus the incoming momentum $p_{in}$ of the dark matter particle equals the outgoing momentum $p_{out} \equiv p$. The NLO amplitude consists of the LO amplitude $\mathcal{A}^{LO}$, the virtual vertex corrections $\mathcal{A}^{VC}$ and the counterterm $\mathcal{A}^{CT}$. In the limit of zero momentum transfer the LO amplitudes for the upper vertex topology read $(i = 1, 2)$

$$i\mathcal{A}_{h_i}^{LO} = C_{\chi\chi h_i} C_{qqh_i} \frac{1}{m_{h_i}^2} \bar{u}(p) u(p)\,, \tag{44}$$

with $C_{\chi\chi h_i}$ given in Eq. (30), the Higgs $h_i$ coupling to a quark pair given by

$$C_{qqh_i} = -\frac{g m_q}{2 m_W} \frac{R_{\alpha,i2}}{\sin\beta} \tag{45}$$

and $u(\bar{u})$ denoting the spinor of the (anti-)quark. The counterterm amplitudes read

[3] For consistency, we do not include any other QCD corrections as *e.g.* the approximate approaches suggested in [30–32]. They would necessarily be incomplete. Together with the missing mixed EW-QCD contributions, this would not allow us to a properly quantify the inclusion of the NLO EW effects on the cross section which we are interested in this paper.

$$i\mathcal{A}^{CT}_{h_1} = \frac{C_{qqh_1}}{m^2_{h_1}}\left(\frac{1}{2}(C_{\chi\chi h_2}\delta Z_{h_2h_1} + C_{\chi\chi h_1}\delta Z_{h_1h_1}) + C_{\chi\chi h_1}\delta Z_{\chi\chi} + \delta C_{\chi\chi h_1}\right) \tag{46}$$

$$i\mathcal{A}^{CT}_{h_2} = \frac{C_{qqh_2}}{m^2_{h_2}}\left(\frac{1}{2}(C_{\chi\chi h_1}\delta Z_{h_1h_2} + C_{\chi\chi h_2}\delta Z_{h_2h_2}) + C_{\chi\chi h_2}\delta Z_{\chi\chi} + \delta C_{\chi\chi h_2}\right), \tag{47}$$

where the counterterm of the coupling is obtained by varying the trilinear coupling $C_{\chi\chi h_i}$,

$$\delta C_{\chi\chi h_i} = \frac{\partial C_{\chi\chi h_i}}{\partial m_W}\delta m_W + \frac{\partial C_{\chi\chi h_i}}{\partial \alpha}\delta\alpha + \frac{\partial C_{\chi\chi h_i}}{\partial \beta}\delta\beta + \frac{\partial C_{\chi\chi h_i}}{\partial g_2}\delta g_2 + \frac{\partial C_{\chi\chi h_i}}{\partial \lambda_7}\delta\lambda_7 + \frac{\partial C_{\chi\chi h_i}}{\partial \lambda_8}\delta\lambda_8. \tag{48}$$

Therefore the NLO amplitude at zero momentum transfer is given by

$$i\mathcal{A}^{NLO}_{h_i} = i\mathcal{A}^{LO}_{h_i} + i\mathcal{A}^{VC}_{h_i} + i\mathcal{A}^{CT}_{h_i} \tag{49}$$

#### 4.1.1. Mediator corrections

To obtain the Wilson coefficient from the mediator corrections the one-loop corrections to the propagator and the corresponding counterterms need to be determined. They can be expressed in terms of the renormalized one-loop propagator $(i, j = 1, 2)$

$$\Delta_{h_ih_j} = -\frac{\hat{\Sigma}_{h_ih_j}(p^2 = 0)}{m^2_{h_i}m^2_{h_j}}, \tag{50}$$

with the renormalised self-energy matrix

$$\begin{pmatrix} \hat{\Sigma}_{h_1h_1} & \hat{\Sigma}_{h_1h_2} \\ \hat{\Sigma}_{h_2h_1} & \hat{\Sigma}_{h_2h_2} \end{pmatrix} \equiv \hat{\Sigma}(p^2) = \Sigma(p^2) - \delta m^2 - \delta T + \frac{\delta Z}{2}\left(p^2 - \mathcal{M}^2\right) + \left(p^2 - \mathcal{M}^2\right)\frac{\delta Z}{2}, \tag{51}$$

with $\delta T$ denoting the tadpole counterterm matrix and $\mathcal{M} \equiv m^2_{h_i}\delta_{ij}$ the diagonal mass matrix. The details of the calculation can be found in [7]. Here we just note that the self-energies receive extra contributions relative to the complex singlet extension in [7] because there are new scalars in the loop from the second doublet.

### 4.2. Lower vertex corrections

The lower vertex corrections are also calculated exactly as in [7]. The difference is again the contribution of the new scalar particles in the loop. However from the point of view of the renormalization procedure nothing changes. A very detailed discussion on the different problems arising in this calculation is presented in our Ref. [9]. Of particular importance is the treatment of infrared divergences and the discussion on the heavy quark contributions to the process.

#### 4.2.1. Box diagrams

Finally, the calculation of the box corrections is also discussed in detail in our previous works, Refs. [7–9] and again was shown to be one order of magnitude smaller than the main contribution.

## 5. Results and discussion

One of the Higgs bosons, either $h_1$ or $h_2$, is the SM-like Higgs boson with a mass of 125.09 GeV [33]. The other CP-even Higgs can be lighter or heavier than the SM-like Higgs boson. The points presented in the scatter plots were generated using `ScannerS` [34,35] where the most relevant experimental and theoretical constraints were taken into account. `ScannerS` checks if the potential is bounded from below, that there is a global minimum and that perturbative unitarity holds. Agreement with the electroweak precision measurements at the $2\sigma$ level is enforced using the $S, T, U$ [36,37] parameters. Collider bounds from Tevatron, LEP and LHC are encoded in `HiggsBounds 5.6.0` [38] and `HiggsSignals 2.3.1` [39]. We ask for a 95% confidence level agreement using the exclusion limits for all available searches for non-standard Higgs bosons, including Higgs invisible decays. Branching ratios are calculated using `AnyHdecay 1.1.0` [35]. The code includes the Higgs decay widths for the N2HDM `N2HDECAY` [40], with state-of-the art higher-order QCD corrections. The code `N2HDECAY` is based on the implementation of the N2HDM in `HDECAY` [41,42]. All EW radiative corrections in `HDECAY` are turned off for consistency.

The DM relic abundance is calculated using `MicrOMEGAs` [43], and a bound on its value is set by the current experimental result $(\Omega h^2)^{\text{obs}}_{\text{DM}} = 0.1186 \pm 0.002$ from the Planck Collaboration [44]. We require the calculated relic abundance to be equal or below its experimental central value plus $2\sigma$, that is, we allow the DM not to saturate the relic density and therefore define a DM fraction

$$f_{\chi\chi} = \frac{(\Omega h^2)_\chi}{(\Omega h^2)^{\text{obs}}_{\text{DM}}}, \tag{52}$$

where $(\Omega h^2)_\chi$ stands for the calculated DM relic abundance in our model. As for direct detection, the PandaX-4T and XENON1T experiments provide the most stringent upper bound on the spin-independent DM nucleon scattering.

The ranges of the input parameters for the scan are shown in Table 1. $m_\Phi$ denotes the masses of $\Phi = h_i, A, H^\pm$, where $h_i$ is the non-125 GeV Higgs. Note that the constraints are applied and therefore the allowed parameter space will be a small fraction of the initial space. In Fig. 2 we present a scatter plot of the $K$-factor, defined as $K = \sigma_{NLO}/\sigma_{LO}$, as a function of the $\sigma_{LO}$ DM-nucleon spin-independent

**Table 1**
Input parameters for the DSP of the N2HDM scan, all parameters varied independently between the given minimum and maximum values. The SM-like Higgs boson mass is set $m_h = 125.09$ GeV and the SM VEV $v = 246.22$ GeV. $m_\Phi$ denotes the masses of $\Phi = h_i, A, H^\pm$. The parameter $\lambda_6$ does not play any role for our computation.

| | $m_\Phi$ [GeV] | $m_\chi$ [GeV] | $\tan\beta$ | $\alpha$ | $\lambda_{7,8}$ |
|---|---|---|---|---|---|
| min | 50 | 1 | 1 | $-\frac{\pi}{2}$ | $-4\pi$ |
| max | 1000 | 1000 | 30 | $\frac{\pi}{2}$ | $4\pi$ |

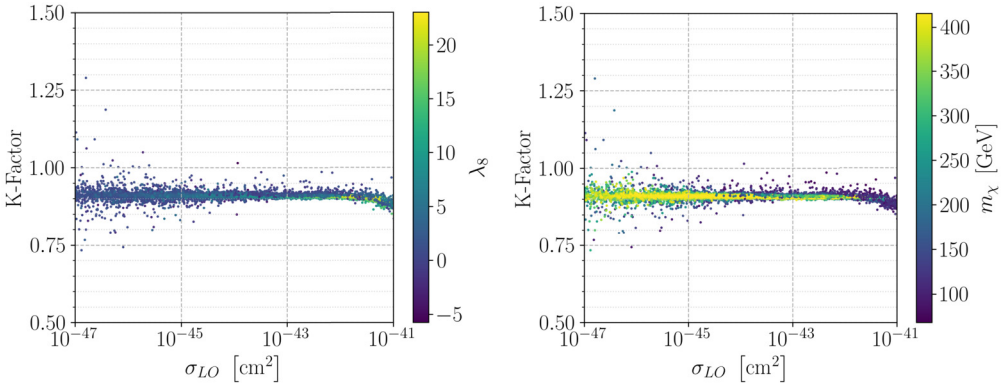


**Fig. 2.** Scatter plot showing the $K$-factor as a function of the $\sigma_{LO}$ DM-nucleon spin-independent cross section. In the left panel we show the behaviour with $\lambda_8$ in the colour bar while in the right panel the DM mass is now shown in the colour bar.

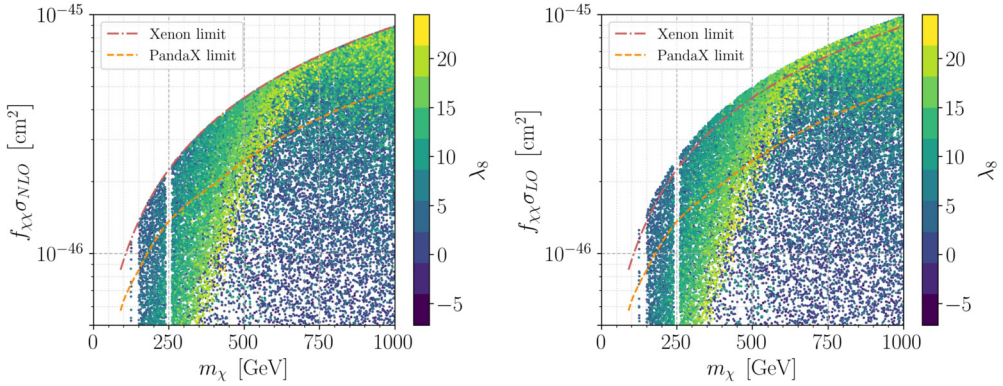


**Fig. 3.** Scatter plot showing the SI cross section, including the correction factor $f_{\chi\chi}$, at NLO (left) and LO (right) compared to the PandaX-4T limit (orange line) and XENON-1T limit (red line), as a function of the DM mass. The colour bar shows the dependence on the parameter $\lambda_8$.

cross section. In the left panel we show the behaviour with $\lambda_8$ in the colour bar while in the right panel the DM mass is shown in the colour bar.

Both the PandaX-4T and the XENON1T experiments set an upper limit on the cross section of $10^{-45}$ cm$^2$ valid for any value of the DM mass (the limit is stronger for smaller DM masses). Therefore, in the region of interest it is clear that the correction is very stable with the bulk of the points just below 0.94 (*note that we have not applied the direct detection bounds in* Fig. 2). The largest value of the correction yields a $K$-factor close to $K = 1.26$ and the lowest value of $K$ is just below 0.75. Hence the correction is stable and there is in general a slight decrease of the cross section at NLO. We have also checked that in the region of interest none of the free parameters play a special role in the $K$-factor values.

In Fig. 3 we now show the DM-nucleon cross section including the correction factor $f_{\chi\chi}$, at NLO (left) and LO (right) compared to the PandaX-4T (orange line) and XENON1T limit (red line), as a function of the DM mass. The points shown are such that they are all below the XENON1T line at NLO as can be seen in the left plot. In the right plot we show that some of the points would not comply with XENON1T limit if calculated at LO. The same conclusions apply to the XENON1T line.

## 6. Conclusions

We have calculated the spin-independent DM-nucleon scattering cross section for the DSP of the N2HDM including higher-order corrections. One of the main goals of this work was to check if the parameter space of the model compatible with the most important theoretical and experimental constraints would give rise to large and/or unstable higher-order corrections. We found that in this model the corrections are stable with a $K$-factor close to one for most of the parameter scenarios. The reason behind this result is that the main corrections come from the upper vertex, mediator and lower vertex, where the diagrams are similar to the ones in the SM extended by a complex singlet field (CxSM). In the CxSM, although the LO cross section turns out to be negligible due to a peculiar Feynman diagram cancellation, the NLO corrections are quite stable as discussed in [5–7]. The same is true for the vector dark matter (VDM) model discussed

in [8,9]. For the VDM the LO cross section is not negligible and the $K$-factor is quite stable and close to one, except for large values of the dark gauge coupling.

Still, in the model discussed in this work, there are new particles in the loops, like for instance in the case of the CP-even self-energies which contribute to the mediator correction, one could in principle expect sizeable corrections which is not the case. The masses and couplings in this model are already very constrained by the LHC results but a such a stable result could not be anticipated.

From the phenomenological point of view the overall conclusions are the following. The NLO corrections can increase the LO results to values where the XENON1T experiment becomes sensitive to the model, or to values where the model is even excluded due to cross sections values above the XENON1T limit. But the reverse is also true even if not as common. Parameter points that might be rejected at LO may render the model viable when NLO corrections are included. We conclude that as a first approximation the LO cross section is a very good approximation but if a DM candidate is detected NLO corrections should be taken into account in order to either validate or exclude the model.

## Declaration of competing interest

The authors declare that they have no known competing financial interests or personal relationships that could have appeared to influence the work reported in this paper.

## Data availability

Data will be made available on request.

## Acknowledgements

RS is supported by FCT under contracts UIDB/00618/2020, UIDP/00618/2020, PTDC/FIS-PAR/31000/2017, CERN/FISPAR /0002/2017, CERN/FIS-PAR/0014/2019. The work of MM is supported by the BMBF-Project 05H21VKCCA.

## Appendix A. Numerical values for the parameters

In this appendix we present the numerical values of the parameters used in the calculation of the cross sections. The SM input parameters are [45]

$$\begin{aligned} &m_u = 0.19\ \text{GeV}, && m_c = 1.4\ \text{GeV}, && m_t = 172.5\ \text{GeV}, \\ &m_d = 0.19\ \text{GeV}, && m_s = 0.19\ \text{GeV}, && m_b = 4.75\ \text{GeV}, \\ &m_e = 0.511\ \text{MeV}, && m_\mu = 105.658\ \text{MeV}, && m_\tau = 1.777\ \text{GeV}, \\ &m_W = 80.398\ \text{GeV}, && v = 246\ \text{GeV}, \\ &m_Z = 91.188\ \text{GeV}. \end{aligned} \tag{53}$$

The $SU(2)$ gauge coupling $g$ and the Weinberg angle are calculated as

$$g = 2m_W/v = 0.653\,, \qquad \sin\theta_W = m_W/m_Z = 0.472\,. \tag{54}$$

The nucleon cross section is calculated for the proton, meaning $\sigma \equiv \sigma_p$, and the mass of the proton is $m_p = 0.938$ GeV.

The nuclear matrix elements for the proton have the following values [27,28]

$$\begin{aligned} &f_u^p = 0.01513\,, && f_d^p = 0.0191\,, && f_s^p = 0.0447\,, \\ &f_g^p = 0.92107\,, \\ &u^p(2) = 0.22\,, && c^p(2) = 0.019\,, \\ &\bar{u}^p(2) = 0.034\,, && \bar{c}^p(2) = 0.019\,, \\ &d^p(2) = 0.11\,, && s^p(2) = 0.026\,, && b^p(2) = 0.012\,, \\ &\bar{d}^p(2) = 0.036\,, && \bar{s}^p(2) = 0.026\,, && \bar{b}^p(2) = 0.012\,, \end{aligned} \tag{55}$$

and no uncertainties in the determination of these nuclear matrix elements were taken into account.

## References

[1] PandaX-4T collaboration, Y. Meng, et al., Dark matter search results from the PandaX-4T commissioning run, Phys. Rev. Lett. 127 (2021) 261802, arXiv:2107.13438.
[2] XENON collaboration, E. Aprile, et al., First dark matter search results from the XENON1T experiment, Phys. Rev. Lett. 119 (2017) 181301, arXiv:1705.06655.
[3] XENON collaboration, E. Aprile, et al., Dark matter search results from a one tonne×year exposure of XENON1T, arXiv:1805.12562.
[4] C. Gross, O. Lebedev, T. Toma, Cancellation mechanism for dark-matter–nucleon interaction, Phys. Rev. Lett. 119 (2017) 191801, arXiv:1708.02253.
[5] D. Azevedo, M. Duch, B. Grzadkowski, D. Huang, M. Iglicki, R. Santos, One-loop contribution to dark-matter-nucleon scattering in the pseudo-scalar dark matter model, J. High Energy Phys. 01 (2019) 138, arXiv:1810.06105.
[6] K. Ishiwata, T. Toma, Probing pseudo Nambu-Goldstone boson dark matter at loop level, J. High Energy Phys. 12 (2018) 089, arXiv:1810.08139.
[7] S. Glaus, M. Mühlleitner, J. Müller, S. Patel, T. Römer, R. Santos, Electroweak corrections in a pseudo-Nambu Goldstone dark matter model revisited, J. High Energy Phys. 12 (2020) 034, arXiv:2008.12985.

[8] S. Glaus, M. Mühlleitner, J. Müller, S. Patel, R. Santos, Electroweak corrections to dark matter direct detection in a vector dark matter model, J. High Energy Phys. 10 (2019) 152, arXiv:1908.09249.
[9] S. Glaus, M. Mühlleitner, J. Müller, S. Patel, R. Santos, NLO corrections to vector dark matter direct detection – an update, in: 19th Hellenic School and Workshops on Elementary Particle Physics and Gravity, vol. 5, 2020, arXiv:2005.11540.
[10] D. Azevedo, M. Duch, B. Grzadkowski, D. Huang, M. Iglicki, R. Santos, Testing scalar versus vector dark matter, Phys. Rev. D 99 (2019) 015017, arXiv:1808.01598.
[11] I. Engeln, P. Ferreira, M.M. Mühlleitner, R. Santos, J. Wittbrodt, The dark phases of the N2HDM, J. High Energy Phys. 08 (2020) 085, arXiv:2004.05382.
[12] I. Engeln, Phenomenological comparison of the dark phases of the next-to-two-higgs-doublet model, Master's thesis.
[13] C.-Y. Chen, M. Freid, M. Sher, Next-to-minimal two Higgs doublet model, Phys. Rev. D 89 (2014) 075009, arXiv:1312.3949.
[14] M. Mühlleitner, M.O.P. Sampaio, R. Santos, J. Wittbrodt, The N2HDM under theoretical and experimental scrutiny, J. High Energy Phys. 03 (2017) 094, arXiv:1612.01309.
[15] M. Mühlleitner, M.O.P. Sampaio, R. Santos, J. Wittbrodt, Phenomenological comparison of models with extended Higgs sectors, J. High Energy Phys. 08 (2017) 132, arXiv:1703.07750.
[16] P.M. Ferreira, M. Mühlleitner, R. Santos, G. Weiglein, J. Wittbrodt, Vacuum instabilities in the N2HDM, J. High Energy Phys. 09 (2019) 006, arXiv:1905.10234.
[17] M. Krause, D. Lopez-Val, M. Muhlleitner, R. Santos, Gauge-independent renormalization of the N2HDM, J. High Energy Phys. 12 (2017) 077, arXiv:1708.01578.
[18] J. Fleischer, F. Jegerlehner, Radiative corrections to Higgs decays in the extended Weinberg-Salam model, Phys. Rev. D 23 (1981) 2001–2026.
[19] M. Krause, M. Muhlleitner, R. Santos, H. Ziesche, Higgs-to-Higgs boson decays in a 2HDM at next-to-leading order, Phys. Rev. D 95 (2017) 075019, arXiv:1609.04185.
[20] L. Altenkamp, S. Dittmaier, H. Rzehak, Renormalization schemes for the two-Higgs-doublet model and applications to $h \to WW/ZZ \to 4$ fermions, J. High Energy Phys. 09 (2017) 134, arXiv:1704.02645.
[21] A. Denner, S. Dittmaier, J.-N. Lang, Renormalization of mixing angles, J. High Energy Phys. 11 (2018) 104, arXiv:1808.03466.
[22] M. Krause, M. Mühlleitner, ewN2HDECAY - a program for the calculation of electroweak one-loop corrections to Higgs decays in the next-to-minimal two-Higgs-doublet model including state-of-the-art QCD corrections, arXiv:1904.02103.
[23] D. Azevedo, P. Gabriel, M. Muhlleitner, K. Sakurai, R. Santos, One-loop corrections to the Higgs boson invisible decay in the dark doublet phase of the N2HDM, J. High Energy Phys. 10 (2021) 044, arXiv:2104.03184.
[24] A. Pilaftsis, Resonant CP violation induced by particle mixing in transition amplitudes, Nucl. Phys. B 504 (1997) 61–107, arXiv:hep-ph/9702393.
[25] S. Kanemura, Y. Okada, E. Senaha, C.P. Yuan, Higgs coupling constants as a probe of new physics, Phys. Rev. D 70 (2004) 115002, arXiv:hep-ph/0408364.
[26] J. Hisano, R. Nagai, N. Nagata, Effective theories for dark matter nucleon scattering, J. High Energy Phys. 05 (2015) 037, arXiv:1502.02244.
[27] J. Hisano, K. Ishiwata, N. Nagata, Direct search of dark matter in high-scale supersymmetry, Phys. Rev. D 87 (2013) 035020, arXiv:1210.5985.
[28] R.D. Young, A.W. Thomas, Octet baryon masses and sigma terms from an SU(3) chiral extrapolation, Phys. Rev. D 81 (2010) 014503, arXiv:0901.3310.
[29] M.A. Shifman, A.I. Vainshtein, V.I. Zakharov, Remarks on Higgs boson interactions with nucleons, Phys. Lett. B 78 (1978) 443–446.
[30] L. Vecchi, WIMPs and un-naturalness, arXiv:1312.5695.
[31] J. Hisano, K. Ishiwata, N. Nagata, QCD effects on direct detection of wino dark matter, J. High Energy Phys. 06 (2015) 097, arXiv:1504.00915.
[32] J. Ellis, N. Nagata, K.A. Olive, Uncertainties in WIMP dark matter scattering revisited, Eur. Phys. J. C 78 (2018) 569, arXiv:1805.09795.
[33] ATLAS, CMS collaboration, G. Aad, et al., Combined measurement of the Higgs boson mass in $pp$ collisions at $\sqrt{s} = 7$ and 8 TeV with the ATLAS and CMS experiments, Phys. Rev. Lett. 114 (2015) 191803, arXiv:1503.07589.
[34] R. Coimbra, M.O.P. Sampaio, R. Santos, ScannerS: constraining the phase diagram of a complex scalar singlet at the LHC, Eur. Phys. J. C 73 (2013) 2428, arXiv:1301.2599.
[35] M. Mühlleitner, M.O.P. Sampaio, R. Santos, J. Wittbrodt, ScannerS: parameter scans in extended scalar sectors, Eur. Phys. J. C 82 (2022) 198, arXiv:2007.02985.
[36] M.E. Peskin, T. Takeuchi, Estimation of oblique electroweak corrections, Phys. Rev. D 46 (1992) 381–409.
[37] W. Grimus, L. Lavoura, O.M. Ogreid, P. Osland, The oblique parameters in multi-Higgs-doublet models, Nucl. Phys. B 801 (2008) 81–96, arXiv:0802.4353.
[38] P. Bechtle, D. Dercks, S. Heinemeyer, T. Klingl, T. Stefaniak, G. Weiglein, et al., HiggsBounds-5: testing Higgs sectors in the LHC 13 TeV era, Eur. Phys. J. C 80 (2020) 1211, arXiv:2006.06007.
[39] P. Bechtle, S. Heinemeyer, O. Stål, T. Stefaniak, G. Weiglein, *HiggsSignals*: confronting arbitrary Higgs sectors with measurements at the tevatron and the LHC, Eur. Phys. J. C 74 (2014) 2711, arXiv:1305.1933.
[40] I. Engeln, M. Mühlleitner, J. Wittbrodt, N2HDECAY: Higgs boson decays in the different phases of the N2HDM, Comput. Phys. Commun. 234 (2019) 256–262, arXiv:1805.00966.
[41] A. Djouadi, J. Kalinowski, M. Spira, HDECAY: a program for Higgs boson decays in the standard model and its supersymmetric extension, Comput. Phys. Commun. 108 (1998) 56–74, arXiv:hep-ph/9704448.
[42] A. Djouadi, J. Kalinowski, M. Muehlleitner, M. Spira, HDECAY: twenty$_{++}$ years after, Comput. Phys. Commun. 238 (2019) 214–231, arXiv:1801.09506.
[43] G. Belanger, F. Boudjema, A. Pukhov, A. Semenov, micrOMEGAs_3: a program for calculating dark matter observables, Comput. Phys. Commun. 185 (2014) 960–985, arXiv:1305.0237.
[44] Planck collaboration, P.A.R. Ade, et al., Planck 2015 results. XIII. Cosmological parameters, Astron. Astrophys. 594 (2016) A13, arXiv:1502.01589.
[45] LHC Higgs Cross Section Working Group collaboration, S. Dittmaier, et al., Handbook of LHC Higgs cross sections: 1. Inclusive observables, arXiv:1101.0593.